METEOROLOGICAL APPLICATIONS
Meteorol. Appl. **20**: 276–286 (2013)
Published online 7 October 2011 in Wiley Online Library
(wileyonlinelibrary.com) DOI: 10.1002/met.301

RMetS
Royal Meteorological Society

Application of a radar-rainfall uncertainty model to the NWS multi-sensor precipitation estimator products

Emad Habib* and Lingling Qin
Department of Civil Engineering, University of Louisiana at Lafayette, LA 70504, USA

ABSTRACT: Given the increasing interest in using radar-based rainfall estimates in hydrologic studies, efforts are critically needed to assess the applicability of recently-proposed methods that focus on quantitative modelling of radar-rainfall uncertainties. The current study reports on the implementation and assessment of an empirically-based approach (known as product-error driven (PED) method) for modelling uncertainties in radar-based rainfall products. In this study, the PED method is applied to a suite of operational radar-based products produced by the U.S. National Weather Service (NWS) Multi-Sensor Precipitation Estimator (MPE) algorithm. The tested MPE products range from a radar-only product, to other products that include various degrees of mean-field and local bias adjustments and gauge-radar optimal merging procedures. Data from an independent dense rain gauge cluster located in south-west Louisiana is used as a proxy for the unknown surface rainfall rates. The focus is on assessing the transferability of the PED across different radar-rainfall products and geographical regions, and the generality of the distributional and parametric assumptions of the PED method. The study also provides insight on the critical issue of the sampling variability and data requirements that govern the implementation, interpretation and possible future enhancements of the radar-error modelling methods.

KEY WORDS radar; rainfall; uncertainty

Received 14 March 2011; Revised 22 July 2011; Accepted 24 August 2011

1. Introduction

Recent technological and scientific advances in the field of rainfall estimation using weather radars present unprecedented opportunities for providing accurate and timely rainfall information. Weather radars provide many advantages over traditional gauge observations especially in terms of their near real-time extensive spatial coverage and relatively high temporal and spatial resolutions, which can make them highly advantageous for a variety of hydrological and meteorological applications. However, radar-rainfall estimates are uncertain due to a variety of effects such as: hardware calibration, non-uniqueness in the relationship between radar-measured reflectivity and rainfall rate, beam overshooting and partial beam filling, anomalous propagation of the radar beam, and non-uniformity in vertical profiles of reflectivity (see Villarini and Krajewski, 2010b for a recent review). Implications of such uncertainties have been well recognized in several hydrological applications that use radar-rainfall estimates (e.g., Sharif *et al*., 2002; Gourley and Vieux, 2005; Habib *et al*., 2008). While research on uncertainties in radar-rainfall estimates has been going on for many years, quantitative knowledge on the statistical characteristics and the full structure of the estimation error is still at an early stage. Ciach and Krajewski (1999) proposed a framework known as the Error Variance Separation (EVS) method, which focused on the estimation of one aspect (variance) of the error distribution (Young *et al*., 2000; Habib *et al*., 2002; Zhang *et al*., 2007; Mandapaka *et al*., 2009). While EVS is limited to the estimation of the error variance only, Habib *et al*. (2004) developed a more general approach that filters out rain gauge errors and retrieves the bi-variate distribution of radar estimates and the corresponding unknown true surface rainfall. Building on such efforts, and motivated by the need for practical methods for modelling radar-rainfall uncertainties, Ciach *et al*. (2007) proposed a product-driven, empirically-based model (referred to herein as PED) which focuses on modelling the combined sources of uncertainties in radar-rainfall estimates. Similar approaches for modelling the combined radar uncertainties (or total estimation error) have been reported in Germann *et al*. (2009).

The essence of the PED method is based on empirical modelling of the relationship between radar-rainfall estimates and the corresponding true surface rainfall (or its approximation from gauge observations) *via* explicit separation of the radar error into two components: deterministic and random. Both of these components are modelled as a function of the radar-rainfall estimate. In its first application, Ciach *et al*. (2007) demonstrated the implementation of the method for the National Weather Service (NWS) Next Generation Weather Radar (NEXRAD) Digital Precipitation Array (PDA) hourly 4×4 km^2 product in Oklahoma, the United States. Villarini and Krajewski (2009) implemented the PED method for a 2×2 km^2 product from a C-band radar in Great Britain and investigated its performance at different time scales (5–180 min). Other applications of the PED method included development of an ensemble generator of probable true surface rainfall fields (Villarini *et al*., 2009a), analysis of the impact of radar-rainfall uncertainties on rainfall-runoff modelling (Habib *et al*., 2008) flash-flood forecasting (Villarini *et al*., 2010), statistical validation of satellite-based precipitation estimates (Villarini *et al*. (2009b), and scaling properties of rainfall (Mandapaka *et al*., 2010). While the PED methodology provides a promising mechanism for characterizing and

* Correspondence to: E. Habib, Department of Civil Engineering, University of Louisiana at Lafayette, P.O. Box 42991, Lafayette, Louisiana 70504, USA. E-mail: habib@louisiana.edu

modelling radar-rainfall uncertainties, its assumptions, parameter estimation, and transferability to other geographic regions and radar setups warrant further investigations. For example, Villarini and Krajewski (2010a) investigated the sensitivity of the PED method to the selection of the reflectivity-to-rainfall (Z-R) relationship and to an algorithm to discriminate between meteorological and non-meteorological returns. They also suggested an additive formulation of the error in addition to its originally proposed multiplicative form. The current study follows on these efforts focusing on several PED methodological aspects such as: (1) application of the PED method to a widely-used operational radar-based multi-sensor estimation algorithm (MPE), (2) sensitivity of the method to different processing procedures and products within the MPE algorithm, (3) transferability of the PED formulation and functional relationships to other geographical regions different from those in earlier applications, and (4) investigation of the sampling-related effects on the estimation of the PED parameters and relationships. Analysis of these aspects will provide further insight into the generality and sampling requirements of the PED methodology and its underlying assumptions, and more importantly, will guide the development and further enhancements of this and other future methods on uncertainty modelling of radar-rainfall products.

2. Study site and data sources

The current study is performed using surface rainfall observations and radar-rainfall estimates over a 35 km^2 experimental watershed (Isaac-Verot, IV) located in the city of Lafayette in south-west Louisiana (Figure 1). The study area is frequently subject to frontal systems, air-mass thunderstorms, and tropical cyclones with annual rainfall of about 140–155 cm and monthly accumulations as high as 17 cm. The study area is fully within the boundaries of the NWS Lower Mississippi River Forecast Center (LMRFC) where the MPE products are primarily derived from the Lake Charles (KLCH) radar. The KLCH site is ∼120 km from the watershed, where the height of the lowest radar beam is about 1.82 km above the ground surface.

2.1. Multisensor precipitation estimator (MPE) products

The Multisensor Precipitation Estimator (MPE) algorithm is implemented at each NWS River Forecast Center (RFC) and produces a set of seven rainfall hourly products over the nominal 4×4 km^2 HRAP grid that are based on different techniques of gauge and radar adjustment and merging (Seo *et al*., 2010). Except the Gauge-only product, all of the other MPE products start from the hourly gridded Digital precipitation Product (DPA). The DPA is generated by the Precipitation Processing System (PPS) where a power law Z–R relationship is applied to the raw reflectivity data, which are then integrated over time to produce hourly accumulation. In the following, a brief description of each of the MPE seven products is provided, focusing on aspects that are most relevant to the current study.

2.1.1. Radar-only (RMOSAIC)

This product is based on mosaicking of the DPA radar product without any use of gauge observations. The RMOSAIC product is expected to be contaminated with large biases that vary by radar site, season and rainfall regime and, therefore, is rarely used by itself (except in areas with no rain gauges). RMOSAIC serves as the first basis for generating the other MPE products.

2.1.2. Gauge-only (GAGEONLY)

This product is based on optimal interpolation of hourly observations from gauges within the service area of the RFC with some climatic adjustments and corrections (Seo *et al*., 2010). This product is useful in regions with poor radar coverage: however, as expected, its quality and accuracy depends largely on the density of rain gauge networks in the area of interest.

2.1.3. Mean field bias-adjusted radar (BMOSAIC)

BMOSAIC is based on applying a radar-specific, time-dependent bias multiplier factor to each pixel in the DPA radar product (Seo *et al*., 1999). The intent of this product is to adjust for systematic, spatially-uniform, spatially correlated biases that may result from the use of inappropriate Z-R relationships or radar calibration problems.

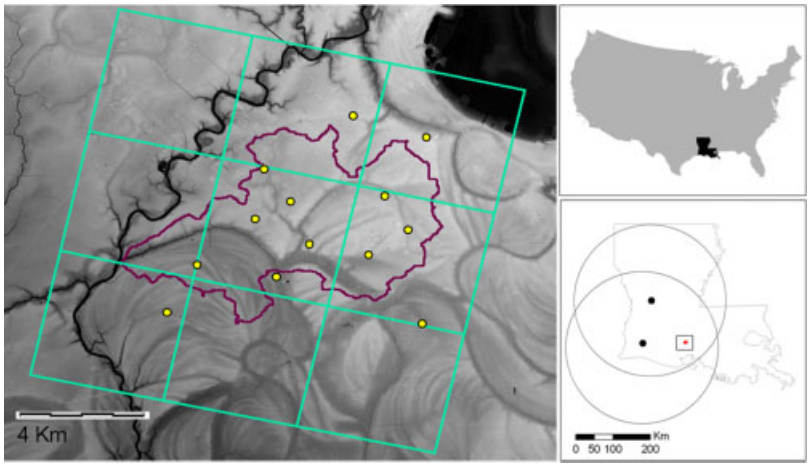

Figure 1. Map of the dense rain gauge network within the Isaac-Verot experimental watershed in Lafayette, Louisiana, the U.S.A. The 4×4 km^2 pixels of the HRAP grid are superimposed over the watershed. The large circles indicate the 200 km umbrellas of the two closest WSR-88D radar stations to the network. ●, Rain Gauge Station. This figure is available in colour online at wileyonlinelibrary.com/journal/met

2.1.4. *Merged multi-sensor mosaic based on BMOSAIC (MMOSAIC)*

This product is based on local merging of the BMOSAIC product with gauge observations. The merging is done at each grid point in the BMOSAIC field by linear distance-based weighting of the BMOSAIC estimate with observations from gauges that are within a user-specified radius of influence. As such, MMOSAIC uses gauge observations both in a mean-field sense (*via* BMOSAIC) and individually and locally within an optimal estimation procedure. The expected outcome is a reduction in both the overall mean error and the random error.

2.1.5. *Local bias-adjusted radar (LMOSAIC)*

Unlike the BMOSAIC, the LMOSAIC product (Seo and Breidenbach, 2002) focuses on spatially non-uniform biases that exist within the RMOSAIC field. The bias adjustment in LMOSAIC is estimated and applied to all HRAP grid points in the RMOSAIC product using hourly rain gauge observations within a fixed user-specified radius of influence measured from each grid point. As such, the bias factors are time and space-varying, and hence the algorithm is computationally demanding.

2.1.6. *Merged multi-sensor mosaic based on LMOSAIC (MLMOSAIC)*

This product is similar to MMOSAIC except that it is based on merging of the local bias-adjusted product (LMOSAIC) with the point rain gauge observations.

2.1.7. *RFC-selected product for hydrologic operations (XMRG)*

This is not a new product in itself, but represents what the RFC forecaster decided to choose in real-time amongst the different MPE products described above to use for operational purposes. Such selection, which can vary from one hour to the next, is driven by the forecaster's own experience and evaluation of the current situation. The product also includes occasional manual corrections by the RFC forecasters.

2.2. Dense rain gauge network

Independent observations from an experimental dense rain gauge network (Figure 1) are used to perform the current analysis. The network is owned and operated by the Civil Engineering Department of the University of Louisiana at Lafayette and is composed of 13 12-in tipping-bucket rain gauge sites, with each site having two gauges located side-by-side (dual-gauge setup). The dual-gauge setup and frequent site maintenance visits and bi-weekly data downloads ensure early detection of malfunctioning problems and continuous data records. To match the resolution of the MPE products, the gauge tips were accumulated to an hourly scale. The period selected for the current analysis is 2 years (2005 and 2006) during which the MPE and gauge observations were available. These 2 years represent average annual rainfall conditions (about 1300 mm or 50 in) with more than 130 events recorded (an event is defined herein as continuous raining period interrupted by no longer than 6 h of no rain and with a rainfall depth of at least 10 mm). Frequent occurrences of sustained intense rain in excess of 25 mm h^{-1} ($\sim$1 in h^{-1}) are observed in the selected study period (see Habib *et al.*, 2009 for a more detailed description of the rain gauge dataset).

3. Approach and methods

3.1. Estimation of approximate true surface areal rainfall

Based on the network spatial arrangement within the study area, two HRAP pixels of the MPE products are covered by multiple gauges (one pixel is covered by six gauges and another pixel is covered by four gauges; Figure 1). Within these two pixels, the inter-gauge distances are in the order of 1–2 km, which is smaller than the correlation distance of hourly rainfall in this area (Habib *et al.*, 2009). Therefore, by averaging observations from multiple gauges within each of the two pixels, a fairly reliable estimate of the unknown true pixel-average surface reference rainfall (which we refer to as R_s) that is not significantly contaminated by the point-to-area errors typically associated with single-gauge observations can be obtained. In the remainder of this study, the estimation error of a certain MPE product is defined as the deviation between MPE estimate and the corresponding R_s value. For consistency, the MPE-R_s samples are based upon paired datasets excluding hours when rainfall was not recorded by R_s or any of the MPE products.

3.2. PED method for radar-rainfall uncertainty modelling

A complete description of the Product-Error-Driven (PED) method is given in Ciach *et al.* (2007) and Villarini and Krajewski (2010a): only a brief overview is provided herein. The PED approach starts with estimating and removing the product overall bias (B_0):

$$B_0 = \frac{\sum_i R_{s,i}}{\sum_i R^*_{r,i}} \tag{1}$$

$$R_{r,i} = B_0 R^*_{r,i} \tag{2}$$

where B_0 is the bias factor, $R_{s,i}$ is the i^{th} hourly surface reference rainfall (obtained by averaging observations from multiple gauges within each pixel), $R^*_{r,i}$ and $R_{r,i}$ are the corresponding hourly radar-product rainfall values (before and after correction for overall bias, respectively). The summation is taken over all hours available during the entire 2 year sample.

After removing the overall bias, the relation between surface rainfall R_s and the radar-product rainfall can be described as a combination of a systematic function (h) and a random component (ε) using two possible formulations, additive and multiplicative:

$$R_s = h(R_r) + \varepsilon_a(R_r) \tag{3}$$

$$R_s = h(R_r)\varepsilon_m(R_r) \tag{4}$$

Both h and ε are functions of the radar-rainfall values. The systematic function characterizes the conditional bias in the radar-rainfall product and can be estimated as a conditional expectation function:

$$h(R_r) = E[R_s | R_r = r_r] \tag{5}$$

where r_r and r_s represent specific values of the random variables R_r and R_s.

The systematic function (h) can now be removed to yield the random component in either the multiplicative or the additive error forms:

$$\varepsilon_{\mathrm{m}}(R_{\mathrm{r}}) = \frac{R_{\mathrm{s}}}{h(R_{\mathrm{r}})} \tag{6}$$

$$\varepsilon_{\mathrm{a}}(R_{\mathrm{r}}) = R_{\mathrm{s}} - h(R_{\mathrm{r}}) \tag{7}$$

After removing the conditional and unconditional biases in R_{r}, it can be reasonably assumed that the conditional means of $\varepsilon_{\mathrm{m}}(R_{\mathrm{r}})$, $E[\varepsilon_{\mathrm{m}}|R_{\mathrm{r}} = r_{\mathrm{r}}]$, and $\varepsilon_{\mathrm{a}}(R_{\mathrm{r}})$, $E[\varepsilon_a|R_r = r_r]$, are equal to 1 and 0, respectively.

The conditional variances of ε_{m} (R_{r}) and ε_{a} (R_{r}) can be expressed as:

$$\sigma^2_{\varepsilon,\mathrm{m}}(r_{\mathrm{r}}) = E[(\frac{R_{\mathrm{s}}}{h(r_{\mathrm{r}})} - 1)^2|R_{\mathrm{r}} = r_{\mathrm{r}}] \tag{8}$$

$$\sigma^2_{\varepsilon,\mathrm{a}}(r_{\mathrm{r}}) = E[(R_{\mathrm{s}} - h(r_{\mathrm{r}}))^2|R_{\mathrm{r}} = r_{\mathrm{r}}] \tag{9}$$

Following Ciach (2003) and Ciach *et al*. (2007), a kernel regression approach is used to obtain a non-parametric estimate of the two conditional statistics, $h(r_{\mathrm{r}})$ *and* σ_ε (r_{r}) using a moving-window averaging formula (see equations (6) and (9) in Ciach *et al*. (2007) and equation (10) in Villarini and Krajewski (2010a)). For a comparison between parametric and non-parametric approaches, the interested reader is pointed to Villarini *et al*. (2008).

To provide further characterization of the distribution of the conditional random error, the PED method also computes the conditional quantiles (q_p) for various levels of probabilities P:

$$\Pr[\varepsilon_{\mathrm{m}}(R_{\mathrm{r}}) \le q_p|R_{\mathrm{r}} = r_{\mathrm{r}}] = P \tag{10}$$

$$\Pr[\varepsilon_{\mathrm{a}}(R_r) \le q_p|R_{\mathrm{r}} = r_{\mathrm{r}}] = P \tag{11}$$

Following the same non-parametric estimation method, weighted-point-counting procedure was used to estimate q_p (see equation 11 in Ciach *et al*. (2007)).

Besides marginal statistics, the PED method includes characterization of spatial and temporal auto-dependencies of the random error using the Pearson's product-moment correlation coefficient. The spatial auto-correlation of the random component is estimated by calculating the correlation between the MPE errors at the two neighbouring multiple-gauge HRAP pixels. The limited spatial coverage of the current gauge network allows for estimating the auto-spatial correlation at one spatial lag only (4 km). The temporal auto-correlations can be computed at various separation time lags (1–6 h) using the random error sample over a single pixel.

3.3. Bootstrap distributions

To assess the impact of sample size on the estimated parameters of the PED method (especially at high rain rates where the sample size is small), their sampling distributions were computed using a bootstrap re-sampling technique. This was achieved by random drawing with replacement from each conditional sample and repeating the calculations of the specific conditional statistic for each of these bootstrap pseudo-samples that had the same size as the original conditional data sample. This re-sampling procedure was repeated 500 times for each conditional sample to deliver stable uncertainty bounds for the derived conditional statistic. The bootstrap distributions are summarized by presenting their 5 and 95% percentiles.

4. Results and discussions

4.1. Overall bias

The overall bias (B_0) was calculated for each MPE product and the results are summarized in Table 1. We also include the corresponding results from Ciach *et al*. (2007), Villarini and Krajewski studies (2009, 2010a). For space limitations, papers are referred to as Ciach and V&K studies, respectively). We calculated the bias over the entire sample (2 years) combining data from the two individual multiple-gauge pixels. Based on the definition of B_0, a value of B_0 smaller (larger) than 1 indicates overestimation (underestimation) by the MPE product. The radar-only product (RMOSAIC) shows a strong overestimation bias ($B_0 = 0.83$). This agrees with the results reported in the Ciach and V&K studies. However, their bias values were significantly lower (0.38–0.73, depending on the selected Z–R relationship). The overall overestimation bias in RMOSAIC was significantly alleviated after removing the mean-field bias in the BMOSAIC product ($B_0 = 0.99$). The next product (MMOSAIC) which optimally merges BMOSAIC with individual gauges does not change the overall bias, which is consistent with the overall intent of MMOSAIC that does not focus on bias improvement. Application of a local bias removal approach (LMOSAIC) instead of the mean-field bias adjustment has introduced an underestimation overall bias ($B_0 = 1.09$). Merging LMOSAIC with individual gauge data (resulting in the MLMOSAIC product) eliminated most of the overall bias ($B_0 = 1.01$).

4.2. Conditional bias

After removing the overall bias, the conditional bias (described by the systematic distortion function, h, Equation (5)) was estimated for each of the MPE products (Figure 2). We limited the conditional analysis for $R_{\mathrm{r}} < 20$ mm h^{-1} to maintain an adequate sample size ($\sim$100 R_{r}–R_{s} pairs). The bootstrap-derived sampling distributions (summarized by the 5 and 95% bounds) of the h function are also presented (only one example is shown for space limitations; other products showed similar distributions). The uncertainty bound of the systematic distortion function is quite narrow for small rain rates (<5 mm h^{-1}) but grows wider with the increase of R_{r} to reach about $\pm$2 mm h^{-1} when $R_{\mathrm{r}} = 20$ mm h^{-1}. Following Ciach *et al*. (2007), a parametric power-law function was fitted to the non-parametric empirical estimates of $h(r_{\mathrm{r}})$:

$$h(r_{\mathrm{r}}) = a_h r_{\mathrm{r}}^{b_h} \tag{12}$$

The resulting fitting coefficients of this function (a_h and b_h) are summarized in Table 1. It is noted that the distortion function of RMOSAIC and MLMOSAIC have an S-shape, which makes the power fitting model less satisfactory. Except the GAGEONLY product, all MPE products have b_h coefficients that are close to 1.0, which indicates a fairly linear relationship between h and R_{r}. The nonlinear features in the distortion function (as reflected in the b_h coefficient) are less obvious than those in Ciach and V&K studies, which indicates a less severe conditional bias in the MPE products.

The distortion function h shows some degree of sensitivity to the product type with MLMOSAIC attaining the lowest conditional overestimation levels especially for the intermediate ranges of R_{r} (10–14 mm h^{-1}). However, the observed differences amongst the various MPE products (except for the

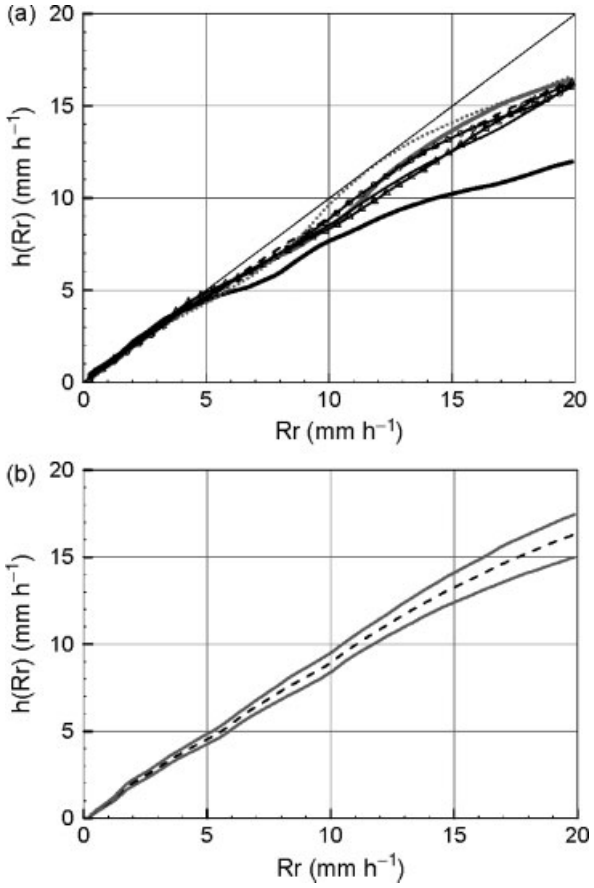

Figure 2. (a) The deterministic distortion (h) as a function of the radar-rainfall rate (R_r) for all MPE products (key: RMOSAIC (solid thick grey line), GAGEONLY (solid thick black line), BMOSAIC (line with triangle symbol), MMOSAIC (dashed line), LMOSAIC (line with circle symbol), MLMOSAIC (dotted line), XMRG (solid thin black line)). (b) The bootstrap 2.5 and 97.5% sampling confidence bounds for the estimated deterministic distortion (shown only for MMOSAIC as an example).

MLMOSAIC) do not seem to be quite significant as they all fall within the 5 and 95% uncertainty bounds (Figure 2). It is also noted that the gauge-only product (GAGEONLY) is characterized by a strong statistically-significant conditional overestimation that continues to deteriorate with the increase of the conditioning R_r value.

4.3. Standard deviation of the random error component

After estimating for the overall bias and the systematic distortion function, we can estimate the R_r-conditioned random component of the MPE errors using the two error formulations: multiplicative ($\varepsilon_m(R_r)$) and additive ($\varepsilon_a(R_r)$). Since the overall and conditional biases were both removed, the mean of ε_m and ε_a can be assumed equal to one and zero, respectively. Their conditional standard deviations ($\sigma_{\varepsilon m}(R_r)$) and ($\sigma_{\varepsilon a}(R_r)$) for each MPE product were then calculated and plotted as a function of R_r (Figures 3 and 4). An example of the bootstrap sampling distributions for one of the MPE products is also shown. Similar to the distortion function, two parametric relationships of the power-law type and the hyperbolic type were fitted to the standard deviation of the multiplicative and additive error, respectively:

$$\sigma_{\varepsilon,m}(r_r) = \sigma_{0\varepsilon,m} + a_{\varepsilon,m} r_r^{b_{\varepsilon,m}} \quad (13)$$

$$\sigma_{\varepsilon,a}(r_r) = a_{\varepsilon,a} r_r^{b_{\varepsilon,a}} \quad (14)$$

The results of the fitting coefficients for the two relationships and for every MPE product are summarized in Table 1 along with the corresponding results from Ciach and V&K studies.

As expected, both standard deviations show strong dependence on the MPE rainfall rates. The standard deviation of the multiplicative error (ε_m) decreases with the increase of R_r while the additive error (ε_a) has a standard deviation that grows with the increase of R_r. The $\sigma_{\varepsilon,m}$ decreases rapidly at small rain rates and then tapers off with the increase of R_r.

Table 1. Values of the overall bias (B_0) and the fitting parameters of the systematic distortion function (h) and the standard deviation of the multiplicative and additive random error for the different products in the MPE algorithm.

	Radar product	Overall bias (B_0)	Systematic distortion function (h)		Standard deviation of random additive error		Standard deviation of random multiplicative error		
			a_h	b_h	$a_{\varepsilon,a}$	$b_{\varepsilon,a}$	$\sigma_{0\varepsilon,m}$	$a_{\varepsilon,m}$	$b_{\varepsilon,m}$
	RMOSAIC	0.83	1.26	0.82	1.34	1.34	0.37	0.70	−0.54
	GAGEONLY	1.02	1.42	0.67	1.74	1.74	0.78	0.52	−0.63
Current study (south-west Louisiana)	BMOSAIC	0.99	1.22	0.85	1.22	1.22	0.43	0.59	−0.63
	MMOSAIC	0.99	1.26	0.82	1.16	1.16	0.33	0.61	−0.48
MPE	LMOSAIC	1.09	1.21	0.84	1.16	1.16	0.24	0.73	−0.44
	MLMOSAIC	1.01	1.25	0.81	1.25	1.25	0.50	0.34	−0.69
	XMRG	1.03	1.30	0.81	1.21	1.21	0.33	0.62	−0.54
Villarini and Krajewski (2009) (south-west England)	C-band Wardon Hill radar	1.26	1.14	0.73	N/A	N/A	0.56	0.09	−1.2
Villarini and Krajewski (2010a) (Central Oklahoma)	NEXRAD (default Z-R)	0.68	1.21	0.87	1.83	1.83	0.00	1.20	−0.25
Ciach *et al*. (2007) (Central Oklahoma)	DPA	0.72	1.23	0.87	N/A	N/A	0.15	1.00	−0.31

The corresponding values from earlier studies are also shown.

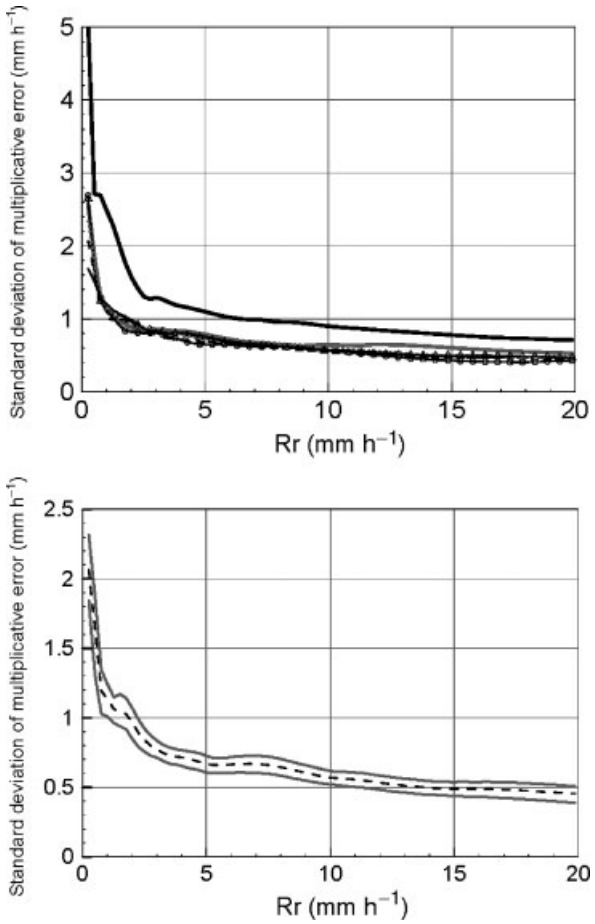

Figure 3. (a) Standard deviation of the random component (multiplicative form; ε_m) for the different MPE products (key: RMOSAIC (solid thick grey line), GAGEONLY (solid thick black line), BMOSAIC (line with triangle symbol), MMOSAIC (dashed line), LMOSAIC (line with circle symbol), MLMOSAIC (dotted line), XMRG (solid thin black line)). (b) The bootstrap 2.5 and 97.5% sampling confidence bounds for the estimated standard deviations (shown only for MMOSAIC as an example).

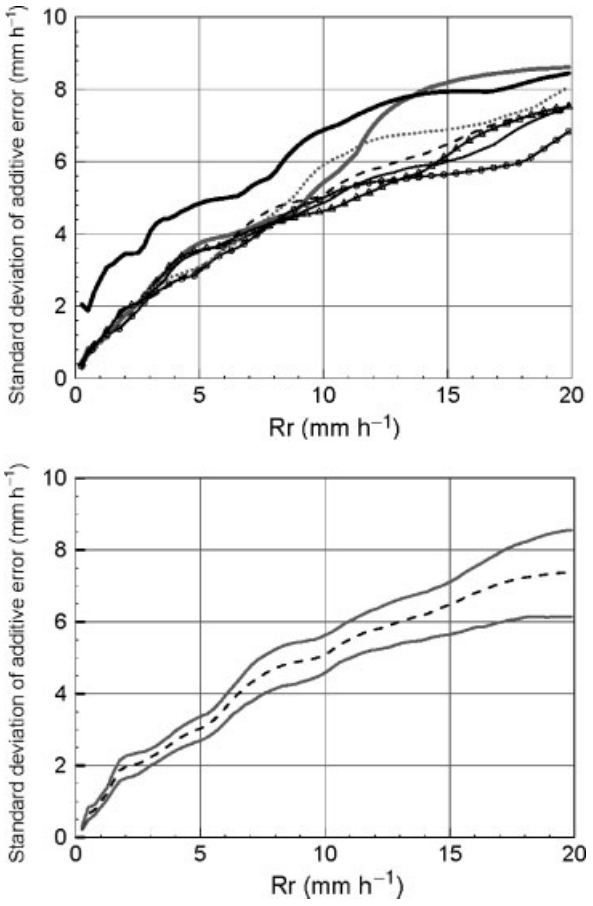

Figure 4. Same as Figure 3 but for the case of the additive form of the error.

An opposite behaviour is associated with $\sigma_{\varepsilon,a}$ which grows systematically with the increase of R_r with some signs of leveling off at larger rain rates. The bootstrap sampling distributions of the two estimated standard deviations have distinctly different behaviours. For small rain rates ($R_r < 2–3$ mm h^{-1}), the uncertainty bound of the estimated standard deviation is fairly wide (narrow) for the multiplicative (additive) error. This is possibly due to that the ratio-nature of the multiplicative error makes it rather volatile to small values of R_r, which is not the case for the additive definition of the error. For medium to large R_r values, $\sigma_{\varepsilon,m}(R_r)$ maintains a fairly uniform width of its sampling distribution, while that of $\sigma_{\varepsilon,a}(R_r)$ gets wider as R_r increases. The degree of product sensitivity of the error standard deviation depends on which error formulation is being used. The standard deviation of the random error in its multiplicative form does not show any noticeable sensitivity to the MPE product. A higher sensitivity is observed for the additive form of the error especially for medium to large rain rates. However, the significance of such sensitivity may not be affirmed given the relatively wide uncertainty bounds in its sampling distribution. It is also observed that moving from a radar-only algorithm (RMOSAIC) to a multi-sensor algorithm with bias-removal and gauge-merging techniques (e.g., MMOSAIC) has resulted in a noticeable reduction in the standard deviation of the multiplicative error especially for relatively large rain rate values ($R_r > 10$ mm h^{-1}). A similar reduction but with less magnitude is also observed with the additive form of the error. While such reductions may not appear highly significant, they are consistent with the intention of applying optimal merging techniques in the MPE algorithm to reduce the random errors in the rainfall estimates.

4.4. Probability distribution of the random error component

To provide further statistical description of the MPE estimation error random component, the empirical quantiles of the random error at different probability levels (p) conditioned on R_r using Equations (10) and (11) (Figures 5 and 6) were calculated. We also estimated the sampling distributions of the empirical quantiles using the bootstrap technique and show some examples in Figure (7) in terms of the 5 and 95% distribution bounds. The quantiles of the additive error have narrow sampling distributions at low and intermediate R_r ranges ($R_r < 10–15$ mm h^{-1}) and becomes wider at large rain rates. On the other hand, the sampling distribution of the multiplicative error quantiles is quite wide for all R_r ranges, especially for the upper quantiles (compare the bounds of $p = 90\%$ to those of $p = 10\%$).

Following Ciach *et al.* (2007) and Villarini and Krajewski (2010a), the possibility of using a Gaussian probability distribution to describe the conditional distribution of both $\sigma_{\varepsilon,m}$ and $\sigma_{\varepsilon,a}$ was assessed. Therefore, the Gaussian quantiles for

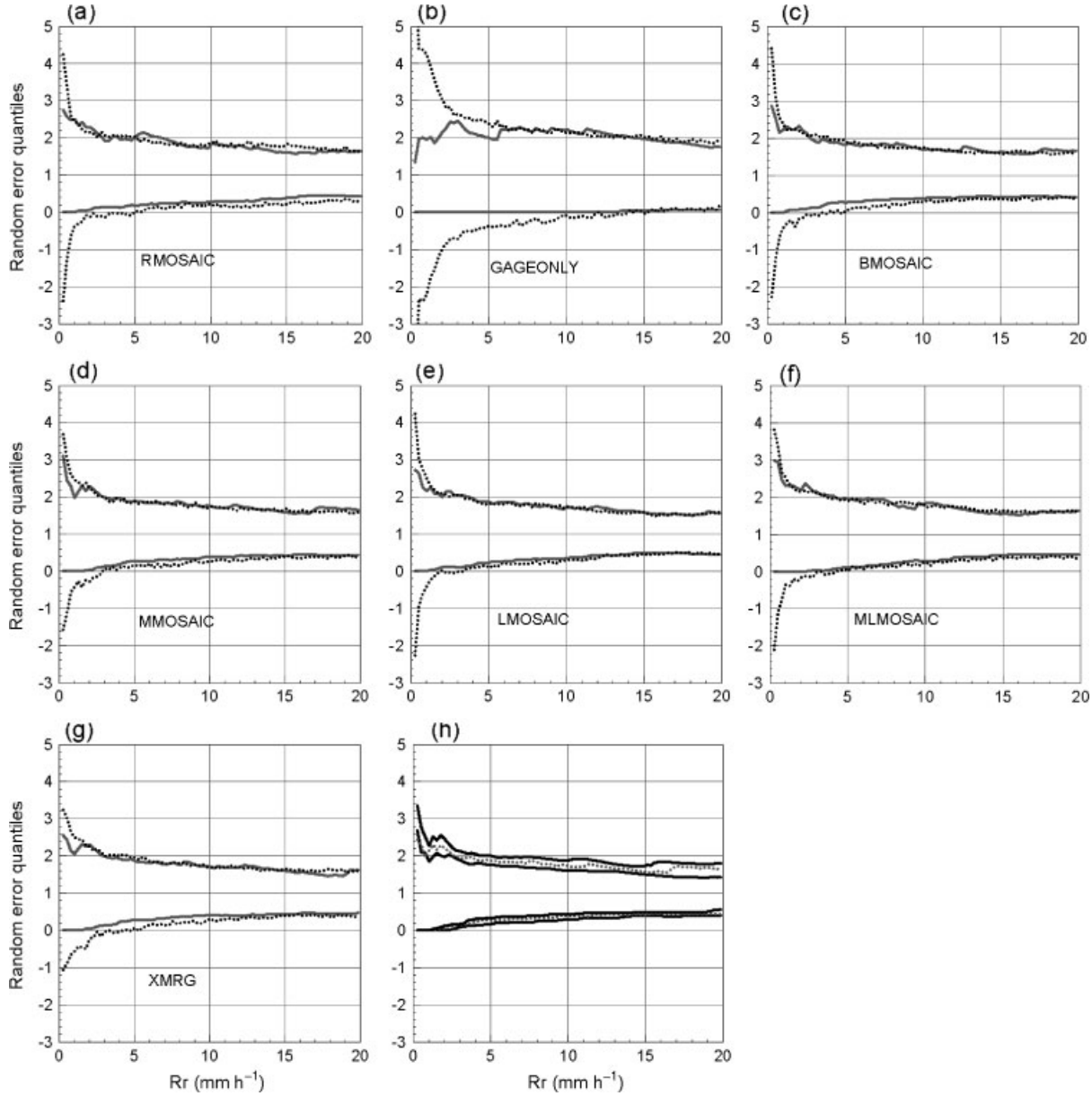

Figure 5. (a–g) Comparison of the empirical (solid line) and the Gaussian theoretical (dotted line) quantiles (10% and 90%) of the random error in its multiplicative form. The Gaussian distribution has mean equal to zero and standard deviation equal to the conditional standard deviation shown in Figure 4. (h) Bootstrap 2.5 and 97.5% sampling confidence bounds of the estimated quantiles (shown only for MMOSAIC as an example).

different probability levels were calculated using a constant mean of 1and 0 for $\sigma_{\varepsilon \mathrm{m}}$ and $\sigma_{\varepsilon \mathrm{a}}$, respectively, and the empirically estimated conditional standard deviations ($\sigma_{\varepsilon,\mathrm{m}}(R_\mathrm{r})$) and ($\sigma_{\varepsilon,\mathrm{a}}(R_\mathrm{r})$). The empirical and Gaussian conditional quantiles are compared *versus* each other for every MPE product (Figures 5 and 6). A good agreement between the empirical and the theoretical Gaussian quantiles is observed for the additive error for all ranges of R_r. The quality of the agreement is consistent across all MPE products. The results of the multiplicative error form shows a clear deviation of the empirical quantiles from the assumed theoretical Gaussian distribution at small rain rates ($R_\mathrm{r} < 2$–3 mm h^{-1}) which indicates that the Gaussian distribution is not suitable for describing the multiplicative error distribution at such rain rates. It is noted that the empirical lower quantiles (e.g., at $p = 10\%$) are bounded by a value of zero due to the definition of the multiplicative error ($R_\mathrm{r} >= 0$). However, the theoretical distribution does not have a lower bound and takes negative values. The agreement is significantly improved for medium and large rain rates independently of the MPE product.

4.5. Spatial and temporal self-correlation of the random error component

Besides the marginal statistical moments (standard deviation and quantiles), the self-correlation characteristics of the random error component are now examined. The spatial auto-correlation of the random error was estimated by calculating the Pearson's product-moment correlation coefficient (ρ) between the MPE errors at the two neighbouring multiple-gauge HRAP pixels. This provides correlation at one single separation distance of 4 km. The results are summarized in Table 2 where the median and the 5 and 95% of the bootstrap sampling distribution of the

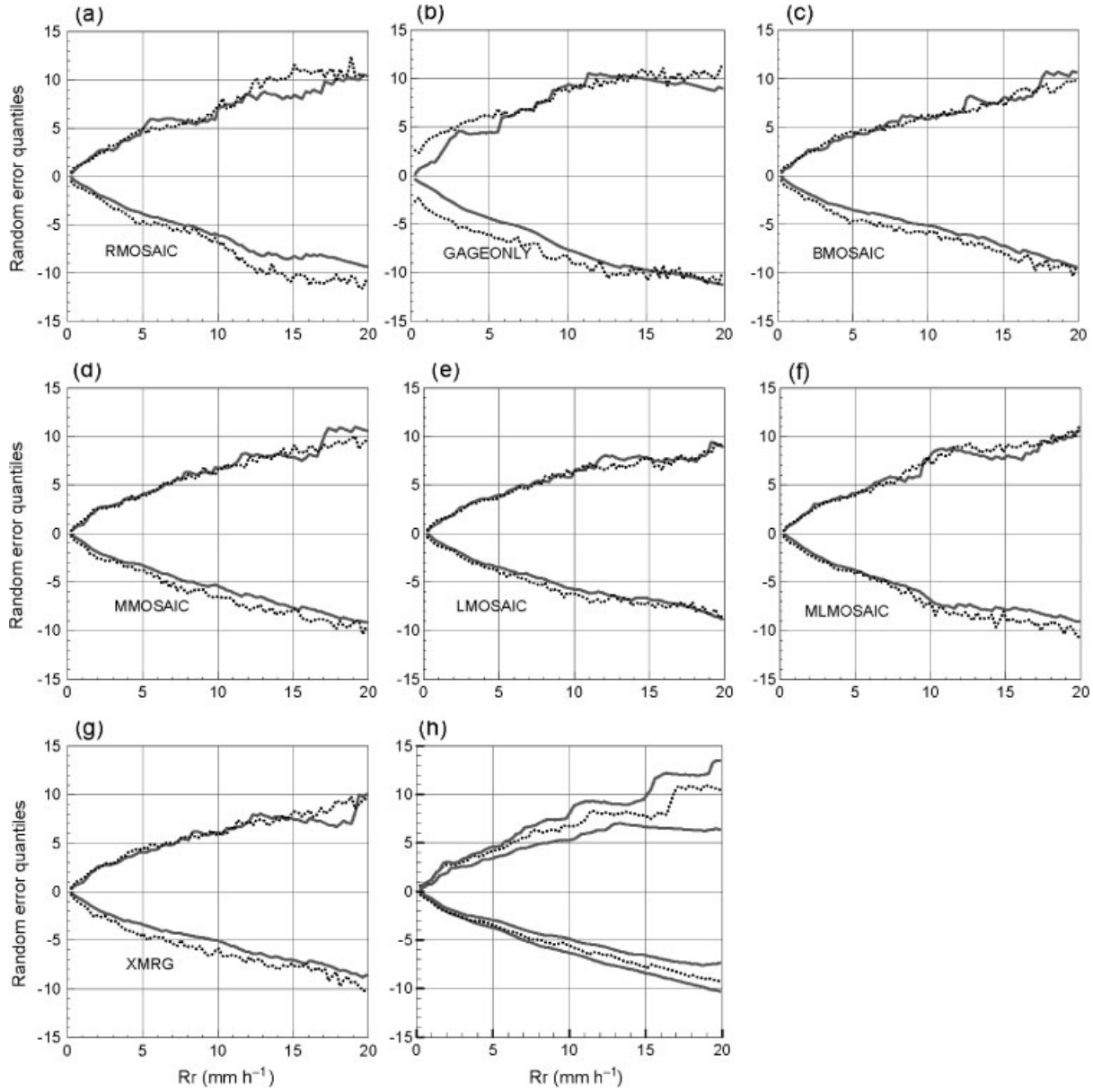

Figure 6. Same as Figure 5 but for the case of the additive error.

estimated spatial correlation coefficients are reported. Temporal auto-correlations were estimated at different separation time lags starting from 1 h and up to 6 h (Figure 7). The results are reported for both formulations of the random error. In general, the random error, either in its multiplicative or additive form, is more correlated in space than in time. At a 4 km lag, the spatial correlation coefficient can be as high as 0.8–0.9 but the temporal correlation does not exceed a value of 0.36 at 1 h lag. The results of the spatial correlations agree quantitatively with those of Ciach and VK studies: however, these studies, especially Ciach *et al*. (2007), report slightly higher temporal auto-correlations. The additive error is highly correlated in space ($\rho = 0.8$–0.9) and shows little sensitivity, if any, to the type of the multi-sensor estimation product. However, the radar-only product (RMOSAIC) has a clearly stronger correlation than the multi-sensor products, which indicates that some of the spatial dependency features in the error field are reduced after applying bias-removal and gauge-merging techniques. Compared to the additive formulation case, the multiplicative error has weaker spatial auto-correlations ($\rho \sim 0.56$) and shows more sensitivity to the different MPE products (e.g., MMOSAIC and XMRG compared to the other MPE products). It is also interesting to note that application of a gauge-radar optimal merging technique (e.g., going from BMOSIAC to MMOSAIC) has resulted in a reduction in the spatial correlation of the multiplicative error. However, this behaviour is not observed in the case of the additive form of the error. The stronger correlation associated with the additive error compared to the multiplicative error is consistent with the VK study. Considering the temporal auto-correlation, the random error correlation seems to be significant only at 1-h separation lag (0.25–0.36) and is much less than the spatial correlation. This reflects weaker self-dependence between the hourly sequences of the random error fields than that attained within the same spatial field. Lower levels of temporal self-correlation are associated with the multiplicative error than the additive error. The degree of sensitivity of the temporal auto-correlations to the type of the MPE product is similar in

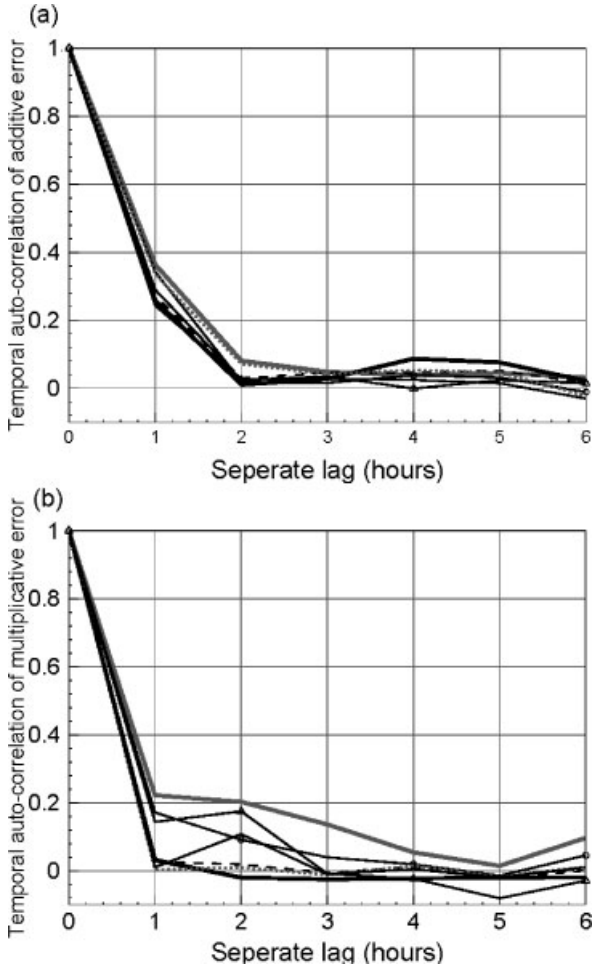

Figure 7. Temporal auto-correlations of the random error component for the case of additive form (a) and the multiplicative form (b).

behaviour to that of the spatial auto-correlation in both error forms where the additive error shows less sensitivity than the multiplicative error (a similar sensitivity behaviour was reported in the VK study). It is also interesting to note that, similar to the spatial correlation, the error of the radar-only product (RMOSAIC) is more self-correlated in time than the other multi-sensor product.

5. Summary, conclusions and final remarks

In this study a product-error driven (PED) radar-rainfall uncertainty modelling methodology was applied the different products of the NWS multi-sensor precipitation (MPE) algorithm. The focus was on some aspects of the PED methodology including: transferability across different radar-rainfall products and geographical regions, and generality or specificity of the PED distributional and parametric assumptions. Some insight on the critical issue of the sampling variability and data requirements that govern the implementation, interpretation and possible future enhancements of the PED method has been provided. It is noted that the sample available to the current study was limited to two full years with more than 130 events. A longer period with a larger sample size may be required to reach more stable statistics and possibly to stratify the sample into different rainfall seasons (e.g., hot *vs* cold) or regimes (e.g., stratiform *vs* convective), for which the model parameters can be better identified. The following is a summary of the main findings along with some concluding remarks for future investigations.

1. All MPE products exhibit a consistent conditional overestimation bias for rain rates beyond 4–5 mm h^{-1}. The systematic distortion function shows some sensitivity to the product type with the local-bias gauge-merged product attaining the lowest conditional overestimation levels.
2. The conditional standard deviation of the random error component (using either formulation, additive or multiplicative) shows strong dependence on rainfall rate. The multiplicative error standard deviation is insensitive to the selection of a certain MPE product. Signs of sensitivity, that cannot be confirmed statistically, are observed for the additive error.
3. The Gaussian probability distribution seems as a valid candidate for modelling the random component of the MPE error especially for the case of the additive error form. A lesser agreement is obtained with the multiplicative error especially for small rain rates.
4. The random error shows strong spatial auto-correlations especially with the additive form of the error (0.8–0.9). The multiplicative form of the error has lesser correlations that are significantly different from zero (up to 0.56). Using a multi-sensor estimation procedure, instead of a radar-only product, seems to reduce some of the spatial coherence in the error fields in both types of error forms. However, the correlation of the additive error does not show any sensitivity to which multi-sensor procedure was used

Table 2. Values of the 4-km spatial auto-correlation coefficients of the multiplicative and additive random error for the different products in the MPE algorithm.

	Radar product	Additive model	Multiplicative model
	RMOSAIC	0.91 (0.81–0.94)	0.56 (0.46–0.74)
	GAGEONLY	0.68 (0.62–0.75)	0.52 (0.24–0.77)
Current study (south-west Louisiana)	BMOSAIC	0.80 (0.74–0.86)	0.46 (0.37–0.63)
	MMOSAIC	0.80 (0.73–0.86)	0.15 (0.14–0.40)
MPE	LMOSAIC	0.81 (0.73–0.87)	0.47 (0.40–0.66)
	MLMOSAIC	0.82 (0.72–0.89)	0.40 (0.26–0.57)
	XMRG	0.81 (0.73–0.87)	0.12 (0.08–0.32)
Villarini and Krajewski (2009) (south-west England)	C-band Wardon Hill radar	N/A	0.57
Villarini and Krakweski (2010) (Central Oklahoma)	NEXRAD (default Z-R)	0.67	0.65
Ciach *et al*. (2007) (Central Oklahoma)	DPA	N/A	0.70

The numbers in the parentheses represent the (5–95%) bounds estimated by the bootstrap re-sampling method. The corresponding values from earlier studies are also shown.

(e.g., using gauges for bias removal only or for further optimal merging). The multiplicative form of the error shows higher sensitivity to the various MPE products.

5. The temporal auto-correlations of the random error appear less significant (<0.4) than the spatial correlations with the additive error being more correlated than the multiplicative error.

While the PED method proposed by Ciach *et al*. (2007) provides a fairly comprehensive approach for modelling radar-rainfall uncertainties, some of its main features may be too general and need further refinements. For example, the most basic element of this method is based on removal of the overall bias. The lumped nature of the overall bias masks out some important details about its composition in a certain product. While the overall bias may be equivalent for any two given MPE products, its sources due to lack of successful detection or false detection can be quite different. A logical refinement of the PED method is to explicitly handle the detection-dependent bias components of the product and develop statistical modelling of each bias component. Further investigations are needed to analyse the complexity added by such refinements and assess its applicability.

In this study, two formulations of the random error component, additive and multiplicative, were evaluated. Both forms seem to offer advantageous features over one another; for example, the standard deviation of the multiplicative error appears to be fairly insensitive to the selection of a specific MPE estimation method and thus offers some degree of product-generality, which is lacking in the case of the additive form of the error. The additive error formulation provides a remarkably good fit to the Gaussian theoretical probability distribution for the entire range of the distribution. The quality of such fit is not as satisfactory with the multiplicative form of the error at low rain rates where the definition of the error makes it inherently bounded by a lower value of zero. The validity of the Gaussian assumption is particularly useful for the purposes of development of statistical generators of probable rainfall fields conditioned on available radar rainfall products (Villarini *et al*., 2009a). At present, the use of one error form over the other is not adopted, but further investigations into their estimation robustness, sampling requirements, and utility under different data and product scenarios are recommended.

The analysis reported in this study provides some insight on the product and regional transferability of the PED uncertainty modelling approach developed earlier by Ciach *et al*. (2007). The current study implemented the uncertainty methodology in a different climatic region (south-west Louisiana *vs* Oklahoma, USA in Ciach *et al*. (2007) and Villarini and Krajewski (2010a), and south-west England in Villarini and Krajewski (2009)) and for a different radar estimation algorithm (MPE *vs* NWS-DPA in Ciach *et al*. (2007) and user-specific Z-R relations in Villarini and Krajewski (2009) and Villarini and Krajewski (2010a)). While the reported results indicate the general applicability of the methodology under these new regional and algorithm conditions, some remarks are worth noting. First, as expected, the overall bias is highly dependent on the specific product under consideration. The radar-only product has an overall bias that is quite different from the multi-sensor versions in the NWS operational MPE algorithm. They are all different from the overall biases reported in the earlier applications (e.g., products based on using different Z-R relationships). The power-law and hyperbolic parametric relationships proposed for describing the systematic distortion function or the standard deviation of the random error seem to be adequate and compatible enough to be used at different regions and estimation algorithms. However, while maintaining similar overall magnitudes, the values of the parameters of such relationships seem to be rather specific and require local estimation. The same applies to the spatial and temporal self-correlation in the error fields. Commonality is observed in the evident strong spatial correlations and fairly weak, but non-negligible temporal correlations. The proposed adoption of a Gaussian distribution as a possible fit for the random error component seems to hold under the regional and data situations of the current study.

An important aspect that the current study addressed is the sampling variability associated with the estimation of the PED different components. A bootstrap approach was implemented to derive the sampling distributions of the empirically-derived error characteristics. The estimation of the systematic distortion function (i.e., the conditional bias) seems to be fairly stable for most rain rates, except at extreme rain rates ($>20-25$ mm h^{-1}) where the sampling distribution becomes relatively wide. As expected, the sampling impact on the standard deviation and the upper quantiles of the random error is more alarming. However, it is interesting to note that the additive error is significantly affected by the sample size limitations at larger rain rates ($R_r >$ 15–20 mm h^{-1}) while the multiplicative error is stable at such ranges but more volatile at small rain rates ($R_r < 3$ mm h^{-1}). Future studies should investigate the performance of the radar uncertainty model in the extreme tails of the distribution, both high and low extremes. Analytical approximations or parameterization of the sampling requirements is important for interpretation, generalization, and setting guidelines for implementation and developments of future radar-error models.

Acknowledgements

This study was funded in part by a sub-award from the Louisiana NASA EPSCoR – DART 2 program, and by the LaSPACE Space Grant.

References

Ciach GJ. 2003. Local random errors in tipping-bucket rain gauge measurements. *Journal of Atmospheric and Oceanic Technology* **20**(5): 752–759.

Ciach GJ, Krajewski WF. 1999. Radar-rain gauge comparisons under observational uncertainties. *Journal of Applied Meteorology* **38**: 1519–1525.

Ciach GJ, Krajewski WF, Villarini G. 2007. Product-error-driven uncertainty model for probabilistic quantitative precipitation estimation with NEXRAD data. *Journal of Hydrometeorology* **8**(6): 1325–1347.

Germann U, Berenguer M, Sempere–Torres D, Zappa M. 2009. REAL – ensemble radar precipitation for hydrology in a mountainous region. *Quarterly Journal of the Royal Meteorological Society* **135**: 445–456.

Gourley JJ, Vieux BE. 2005. Evaluating the accuracy of quantitative precipitation estimates from a hydrologic modeling perspective. *Journal of Hydrometeorology* **2**: 115–133.

Habib E, Aduvala A, Meselhe EA. 2008. Analysis of radar-rainfall error characteristics and implications for streamflow simulations uncertainty. *Journal of Hydrologic Sciences* **53**(3): 568–587.

Habib E, Ciach GJ, Krajewski WF. 2004. A method for filtering out raingauge representativeness errors from the verification distributions of radar and raingauge rainfall. *J. Adv. Water Resour.* **27**(10): 967–980.

Habib E, Krajewski WF. 2002. Uncertainty analysis of the TRMM ground-validation radar-rainfall products: application to the TEFLUN-B field campaign. *Journal of Applied Meteorology* **41**(5): 558–572.

Habib E, Larson B, Graschel J. 2009. Validation of NEXRAD multisensor precipitation estimates using an experimental dense rain gauge network in south Louisiana. *Journal of Hydrology* **373**: 463–478.

Mandapaka PV, Krajewski WF, Ciach GJ, Villarini G, Smith JA. 2009. Estimation of radar – rainfall error spatial correlation. *Advances in Water Resources* **32**: 1020–1030.

Mandapaka PV, Villarini G, Seo B-C, Krajewski WF. 2010. Effect of radar – rainfall uncertainties on the spatial characterization of rainfall events. *Journal of Geophysical Research* **115**: D17110, DOI: 10.1029/2009JD013366.

Seo DJ, Breidenbach JP. 2002. Real-time correction of spatially nonuniform bias in radar rainfall data using rain gauge measurements. *Journal of Hydrometeorology* **3**: 93–111.

Seo DJ, Briedenbach JP, Johnson ER. 1999. Real-time estimation of mean field bias in radar rainfall data. *Journal of Hydrology* **223**: 131–147.

Seo DJ, See A, Delrieu G. 2010. Radar and multisensor rainfall estimation for hydrologic applications. In *Rainfall: State of the Science*. Testik FY, Gebremichael M (eds.). Geophysical Monograph Series, Volume 191. American Geophysical Union: Washington, DC; 288 pp.

Sharif HO, Ogden FL, Krajewski WF, Xue M. 2002. Numerical simulations of radar rainfall error propagation. *Water Resources Research* **38**: 1140, DOI: 10.1029/2001WR000525.

Villarini G, Krajewski WF. 2009. Empirically based modeling of radar-rainfall uncertainties for a C-band radar at different times-scales. *Quarterly Journal of the Royal Meteorological Society* **135**: 1424–1438.

Villarini G, Krajewski WF. 2010a. Sensitivity studies of the models of radar-rainfall uncertainties. *Journal of Applied Meteorology and Climatology* **49**(2): 288–309, DOI: 10.1175/2009JAMC2188.1.

Villarini G, Krajewski WF. 2010b. Review of the different sources of uncertainty in single polarization radar-based estimates of rainfall. *Surveys in Geophysics* **31**: 107–129, DOI: 10.1007/s10712-009-9079-x.

Villarini G, Krajewski WF, Ciach GJ, Zimmerman DL. 2009a. Product-error-driven generator of probable rainfall conditioned on WSR-88D precipitation estimates. *Water Resources Research* W01404, DOI: 10.1029/2008WR006946.

Villarini G, Krajewski WF, Smith JA. 2009b. New paradigm for statistical validation of satellite precipitation estimates: application to a large sample of the TMPA 0.25 degrees 3-hourly estimates over Oklahoma. *Journal of Geophysical Research – Atmospheres* **114**: D12106, DOI: 10.1029/2008JD011475.

Villarini G, Krajewski WF, Ntelekos AA, Georgakakos KP, Smith JA. 2010. Probabilistic forecasting of flash floods: combined effects of uncertainties in radar-rainfall estimates and flash flood guidance. *Journal of Hydrology* **394**(1–2): 275–284.

Villarini G, Serinaldi F, Krajewski WF. 2008. Modeling radar-rainfall estimation uncertainties using parametric and non-parametric approaches. *Advances in Water Resources* **31**(12): 1674–1686.

Young CB, Bradley A, Krajewski W, Kruger A, Morrissey M. 2000. Evaluating NEXRAD multisensor precipitation estimates for operational hydrologic forecasting. *Journal of Hydrometeorology* **1**: 241–254.

Zhang Y, Adams T, Bonta JV. 2007. Subpixel-scale rainfall variability and the effects on separation of radar and gauge rainfall errors. *Journal of Hydrometeorology* **8**: 1348–1363.

